Proceedings of the 9th U.S. National and 10th Canadian Conference on Earthquake Engineering
Compte Rendu de la 9ième Conférence Nationale Américaine et
10ième Conférence Canadienne de Génie Parasismique
July 25-29, 2010, Toronto, Ontario, Canada • Paper No 790

RESPONSE OF CONCRETE GRAVITY DAMS TO SPATIALLY VARYING EARTHQUAKE GROUND MOTIONS

J. Huang[1] and A. Zerva[2]

ABSTRACT

The effect of the spatial variation of earthquake ground motions on the seismic response of concrete gravity dams is investigated. The Koyna Dam is idealized as a two-dimensional finite element model incorporating nonlinearities in the concrete and rock masses, and interactions between the dam, the reservoir, the sediments and the foundation. Sensitivity analyses of the response of the transverse cross section of the dam to the apparent propagation velocity of the seismic excitation are then performed. It is shown that the slower propagating motions yield the highest response and the most severe damage patterns in the structure. Hence, the assumption of uniform seismic excitations at the base of the structures does not lead to a conservative response for concrete gravity dams.

Introduction

The performance of concrete gravity dams in a seismic environment is an important issue of public concern and research attention. Typically, the analysis of their dynamic response to seismic excitations is performed under the assumption that the seismic ground motions over the entire foundation surface area are uniform. It has been shown, however, that the response of structures with large base dimensions, such as bridges, dams and power plants, can be affected by the spatial variation of the seismic excitations, as it induces the quasi-static response of the structures and excites their dynamic response differently than uniform seismic motions (e.g. Zerva 2009). This paper presents a sensitivity analysis of the response of concrete gravity dams subjected to spatially variable seismic excitations incorporating wave passage effects. The approach utilizes the finite element method and considers the coupled dam-reservoir-sediment-foundation system. The following features are included in the computational model: a displacement-based nonlinear dynamic formulation for the dam and the foundation; a pressure-based wave formulation for the reservoir; a coupling procedure for the dam-reservoir-foundation interaction; and consideration of the infinite reservoir and foundation domains. The Koyna Dam in India is then utilized for the sensitivity analysis. The two-dimensional model of the transverse cross section of the dam is subjected to the Koyna Earthquake record that is assumed to propagate on the ground surface with an infinite apparent propagation velocity (uniform

[1]Graduate Student, Dept. of Civil, Architectural and Environmental Engineering, Drexel University, Philadelphia, PA 19104
[2]Professor, Dept. of Civil Architectural and Environmental Engineering, Drexel University, Philadelphia, PA 19104

motions) and two finite ones (4000 and 2000 m/sec). The comparison of the wave passage effect on the structural response is made in terms of crest accelerations, peak stress contours and crack patterns in the body of the dam, and deformations at the dam-foundation interface.

Numerical Formulation

Dam-Reservoir-Sediment-Foundation System

The problem considered in this study consists of a gravity dam with a vertical upstream face, which impounds an infinite reservoir with bottom sediment deposits and rests on a semi-unbounded foundation. A schematic illustration of the coupled dam-reservoir-sediment-foundation system is shown in part (a) of Fig. 1. Part (b) of the figure presents the classification of domains and boundaries, which will be utilized in the description of the mathematical formulation of the dynamic problem presented next.

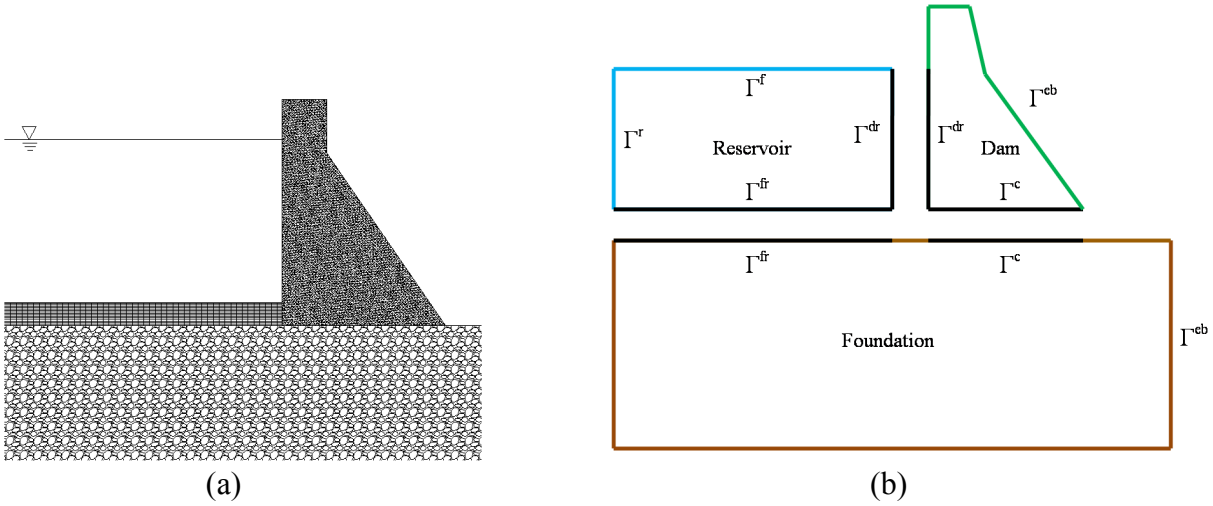

Figure 1. Schematic diagram of dam-reservoir-sediment-foundation system in part (a), and classification of domains and boundaries in part (b).

Modeling of the Fluid Domain and its Boundaries

The differential equation for small motions of an inviscid compressible fluid in the linear range is expressed as:

$$\frac{1}{B^r}\ddot{p}-\frac{1}{\rho^r}\nabla^2 p=0 \qquad (1)$$

in which B^r is the bulk modulus of the fluid in the reservoir, ρ^r its density, p indicates the hydrodynamic pressure in excess of the hydrostatic pressure, overdot denotes time differentiation, and ∇^2 is the Laplacian operator.

The following boundary conditions at the interfaces of the fluid domain (Fig. 2(b)) are then defined:

(i) At the free surface of the reservoir (Γ^f), neglecting the effect of formation of surface waves yields the boundary condition:

$$p=0 \tag{2}$$

(ii) At the truncated boundary of the infinite reservoir (Γ^r), Sandler's nonreflecting boundary (Sandler 1998) is applied:

$$\frac{1}{\rho^r}\frac{\partial p}{\partial n^r}=-\frac{\cos\theta}{\sqrt{B^r\rho^r}}\dot{p} \tag{3}$$

where n^r is the outward normal derivative of the fluid domain and θ is the angle of incidence of the plane waves at the boundary.

(iii) At the dam-reservoir interface (Γ^{dr}), excluding cavitation effects, the continuity condition between the fluid and solid domains leads to:

$$\frac{1}{\rho^r}\frac{\partial p}{\partial n^r}=-\ddot{u}_1^s\times n^r \tag{4}$$

where $\ddot{u}_1^s$ is the acceleration of the dam at the interface.

(iv) At the foundation-reservoir interface (Γ^{fr}), the reservoir bottom material is represented by the following impedance condition:

$$\frac{1}{\rho^r}\frac{\partial p}{\partial n^r}=-\ddot{u}_2^s\times n^r-\frac{1}{\sqrt{B^r\rho^r}}\frac{\left(1-\alpha^r\right)}{\left(1+\alpha^r\right)}\dot{p} \tag{5}$$

where $\ddot{u}_2^s$ is the acceleration of the foundation, and α^r indicates the wave reflection coefficient of the reservoir sediment (Fenves and Chopra 1984).

Modeling of the Solid Domains and their Boundaries

The nonlinear mechanical behavior of the dam concrete and foundation rock is approximated by the damaged plasticity model (Lee and Fenves 1998, Lubliner et al. 1989) and the jointed rock model (Zienkiewicz and Pande 1977), respectively. The dynamic equilibrium equations governing the dam and the foundation response are described by:

$$(\sigma_i^s)_{kj,j}+(f_i^s)_k=\rho_i^s(\ddot{u}_i^s)_k \tag{6}$$

where subscripts i=1 or 2 indicate whether the equation refers to the dam or the foundation, superscript s denotes solid, k,j=1, 2, 3 indicate direction and indicial notation has been utilized over j, σ_i^s is the stress, f_i^s is the body force, ρ_i^s the density, and $\ddot{u}_i^s$ the acceleration.

The surface tractions $\bar{t}$ at the boundaries of the solid domains (Fig. 1(b)) obey the

following constraints:

(i) On the fluid-solid interface ($\Gamma^{rs}=\Gamma^{dr} \cup \Gamma^{fr}$):

$$\bar{t}_i = -p \times n_i^s \tag{7}$$

where p is the fluid pressure and n_i^s the outward normal to the solid.

(ii) On the dam-foundation contact interface (Γ^c):

$$\bar{t}_i = t_i^c \tag{8}$$

where t_i^c are the contact loads.

(iii) On the external boundary of the finite solid domain (Γ^{eb}):

$$\bar{t}_2 = t_2^{eb} \tag{9}$$

where t_2^{eb} are surface tractions excluding fluid pressure and contact loads.

Coupling of the Fluid and Solid Domains

The combination of the fluid and solid virtual work contributions obtained by integrating Eqs. 1 and 6 by parts, the consideration of the boundary conditions defined in Eqs. 2-5 and 7-9, and the standard finite element discretization procedure lead to the following differential equation of motion of the coupled system in matrix form:

$$\begin{bmatrix} [M^s] & 0 \\ [H^{rs}] & [M^r] \end{bmatrix} \begin{bmatrix} \ddot{u}^s \\ \ddot{p} \end{bmatrix} + \begin{bmatrix} f^{int} \\ [K^r]\, p \end{bmatrix} - \begin{bmatrix} f^s + [H^{rs}]^T p + f^c + f^{eb} \\ -[C^r]\, \dot{p} \end{bmatrix} = 0 \tag{10}$$

in which $[M^r]$ and $[M^s]$ refer to the fluid and solid mass matrices, respectively, $[C^r]$ is the fluid damping matrix, $[K^r]$ the fluid stiffness matrix, $[H^{rs}]$ the fluid-solid coupling matrix, f^{int} the solid nonlinear internal force vector, f^s the solid body force vector, f^c the solid contact force vector, f^{eb} the solid surface load vector excluding fluid pressure and contact forces, and superscript T indicates transpose. It is noted that the terms originating from material and radiation damping of the solid domains are implicitly incorporated in f^{int} of Eq. 10.

To appropriately represent the dam-foundation interaction, a contact surface is defined at the dam-foundation interface: The contact interaction in the normal direction is characterized by "hard" contact behavior (Abaqus 2007), and the tangential contact interaction by the Coulomb friction law with an allowable slip (Teckie and Ellingwood 2002). The fluid-structure interactions at the dam-reservoir and foundation-reservoir-sediment interfaces are modeled using a surface-based coupling procedure (Abaqus 2007). The effects of reservoir bottom sediment absorption are incorporated by enforcing the impedance condition specified in Eq. 5 at the foundation-reservoir interface.

Earthquake Input Mechanism

In evaluating the earthquake performance of concrete dams, it has been recognized that the manner in which the seismic excitations are applied to the numerical model may affect the structural response. A commonly utilized approach is to perform first a deconvolution analysis of the original free-field earthquake ground motion to the desired depth. The deconvolved motion is then applied at the base of the foundation and allowed to propagate upward through the foundation. However, the reliability of the results obtained with this approach depends, to a large extent, on the accuracy of the deconvolution process (Leger and Boughoufalah 1989). It is also noted that, in the deconvolution process, it is difficult to incorporate soil material nonlinearities and spatially variable seismic ground motions. An alternative approach is to specify the recorded free-field earthquake acceleration at the dam-foundation interface. The primary drawback of this approach, however, is that the motions at the level of the ground surface, where the free-field accelerations are exerted, are assumed not to be affected by the dam. On the other hand, the advantages of the approach are that deconvolution analyses are avoided and, theoretically, it is possible to specify any spatially varying ground motions as input excitations to the structure. In view of the pros and cons of the earthquake input mechanisms, the present study imposes the free-field earthquake acceleration at the foundation ground surface. Leger and Boughoufalah (1989) observed that this approach and the deconvolution method gave similar results for uniform seismic motions, vertically incident waves, and linear models of the dam and the foundation.

Sensitivity Analysis of Wave Passage Effects

Numerical Model of the Koyna Dam

The Koyna Dam in India is utilized for the sensitivity analysis of the effect of spatially variable excitations on dams. The computational evaluation is performed in Abaqus/Standard (2007). The geometry of a typical non-overflow monolith of the Koyna Dam, which is modified slightly from its real configuration, is illustrated in Fig. 2(a). The finite element model of the dam, presented in Fig. 2(b), is assumed to be under plain strain conditions. The dam and the near-field foundation are modeled by 4-node bilinear continuum plane strain elements. The reservoir is modeled by 4-node bilinear acoustic elements. The reservoir dimensions are 385 m length and 91.75 m depth. The finite foundation domain is 840 m long and 420 m deep; the rock mass contains one set of planes of weakness with joints inclined at an angle of 52.5º. In addition, 4-node linear plain strain infinite elements, as indicated by the open elements in Fig. 2(b), are employed to simulate the far field. The material properties adopted in the analysis are: i) for the concrete: Young's modulus 31027 MPa, Poisson's ratio 0.20, density 2643 kg/m^3, dilation angle 36.31º, compressive initial yield stress 13.0 MPa, compressive ultimate stress 24.1 MPa, tensile failure stress 2.9 MPa; ii) for the rock: Young's modulus 16860 MPa, Poisson's ratio 0.18, density 2701 kg/m^3, cohesion 0.6 MPa, angle of friction 41º; and iii) for the water: bulk modulus 2701 MPa, density 1000 kg/m^3, reservoir sediment reflection coefficient 0.5. Rayleigh stiffness proportional damping is assumed to provide a 3% damping ratio of the first mode of vibration of the linear structure. The dam-reservoir-sediment-foundation system is first subjected to the static loads including gravity and hydrostatic pressure and then to the dynamic earthquake loading.

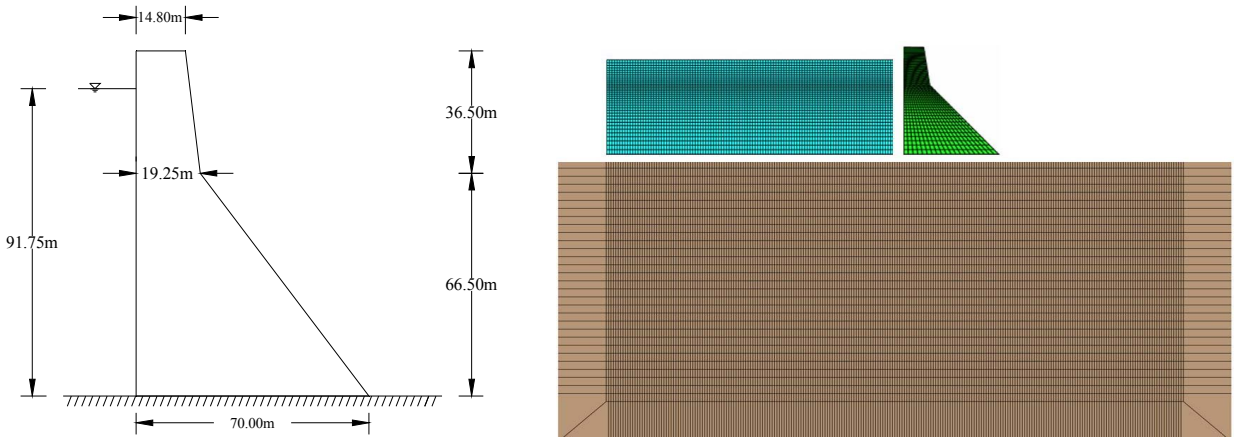

Figure 2. Geometry of a non-overflow monolith of the Koyna Dam in part (a) and finite element modeling of the dam-reservoir-foundation domain in part (b).

Description of Input Excitation

In 1967, the Koyna Dam experienced a magnitude 6.5 earthquake. The event caused considerable damage to the dam, including the development of horizontal cracks on both the upstream and downstream faces of a number of the monoliths. The top subplot of Fig. 3 shows the horizontal component of the Koyna Earthquake record, which will be utilized in the subsequent evaluation. Sensitivity analyses of the response of the dam to spatially varying ground motions are conducted by considering wave passage effects. The spatially variable seismic excitations are modeled by the propagation of horizontally travelling seismic waves with two finite apparent propagation velocities, v_{app}= 2000 and 4000 m/sec, and an infinite one; the last case represents the condition of uniform excitation. The simulated ground motions utilized as input excitations at the rightmost node of the foundation surface for the aforementioned three earthquake loading scenarios are plotted, in descending propagation velocity order, in Fig. 3.

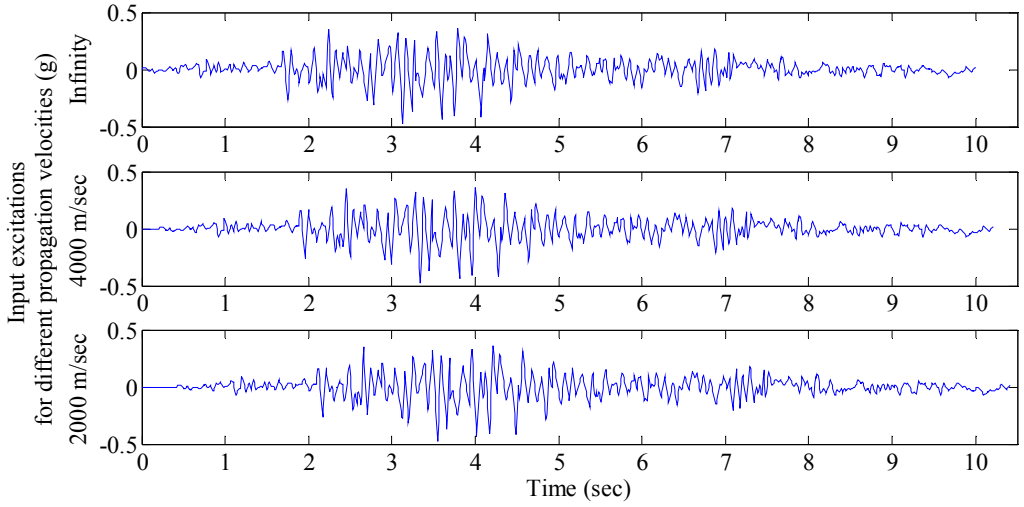

Figure 3. Input excitations at the rightmost node of the foundation surface for different loading scenarios.

Seismic Response Evaluation of the Koyna Dam

The results of the evaluation are presented in the following figures. The horizontal acceleration response at the dam crest for the different ground motion input scenarios is shown in Fig. 4. For uniform ground motions (top subplot), the peak acceleration occurs at 4.159 sec with an amplitude of 1.65 g. For motions propagating with an apparent velocity of 4000 m/sec (middle subplot), the peak response with an amplitude of 1.68 g occurs at 4.267 sec, and for the slower propagating motions (bottom subplot), the peak amplitude of 1.84 g occurs earlier than the other two cases at 3.433 sec. It is noted that the response for all types of excitation is very significant; this may be attributed, in part, to the low value of damping utilized in the evaluation and, also, to the approach for inputting the seismic excitation to the numerical model. The response characteristics for an infinite apparent propagation velocity and a velocity of 4000 m/sec are fairly similar, indicating that, for v_{app}= 4000 m/sec, the excitation travels fast enough so that the time delay in the arrival of the waves throughout the finite domain of the model does not play a considerable role. On the other hand, even though the response acceleration time series for v_{app}= 2000 m/sec appears, at first glance, similar to the other two (Fig. 4), its peak value occurs earlier, and, during the time interval of the larger oscillations (approximately between 3 and 4.5 sec), the amplitude of the response is larger. This suggests that the lower apparent propagation velocity caused additional cracking and sliding of the structure than the faster propagation velocities, thus making the structure more flexible. This observation is further corroborated with the results presented in Figs. 5-8.

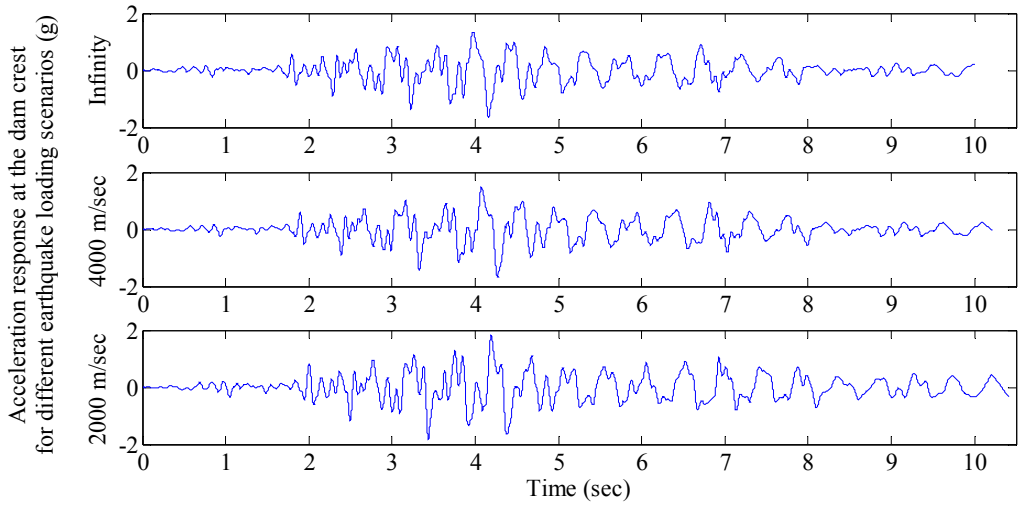

Figure 4. Acceleration response at the dam crest under spatially variable seismic excitations with different apparent propagation velocities.

Part (a) of Figs. 5-7 displays the peak von Mises stress contours occurring in the body of the dam for each input case at a specific time instant. The time instances were selected to be close to the peak amplitude acceleration response for the faster apparent propagation velocities and, from Fig. 4, close to the corresponding peak for the case of v_{app}= 2000 m/sec (i.e. 4.165, 4.279 and 4.401 sec, respectively). At these particular instances, high stress concentrations are observed in the slope transition region on the downstream dam face. It is noted that, during the reversing oscillatory cycles of the response (Fig. 4), high stress concentrations also occur at the

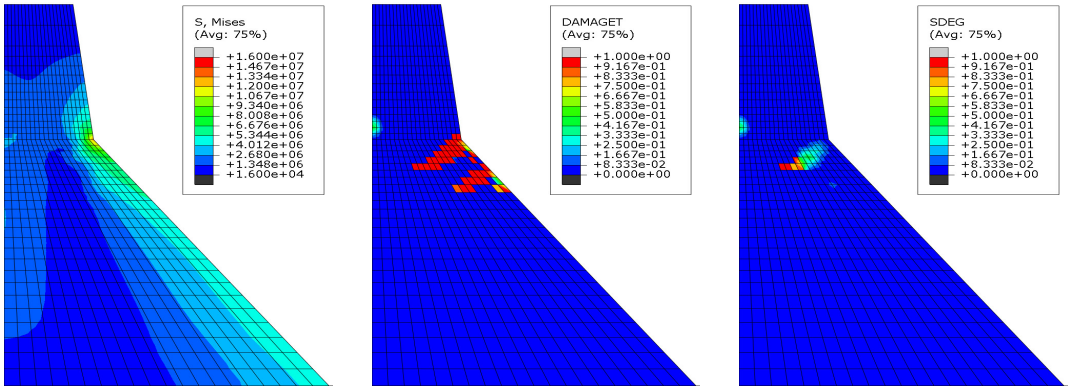

(a) (b) (c)

Figure 5. Peak stress (in Pa) and damage contours of the dam at 4.165 sec for earthquake input with infinite propagation velocity: (a) von Mises stress; (b) DAMAGET; (c) SDEG.

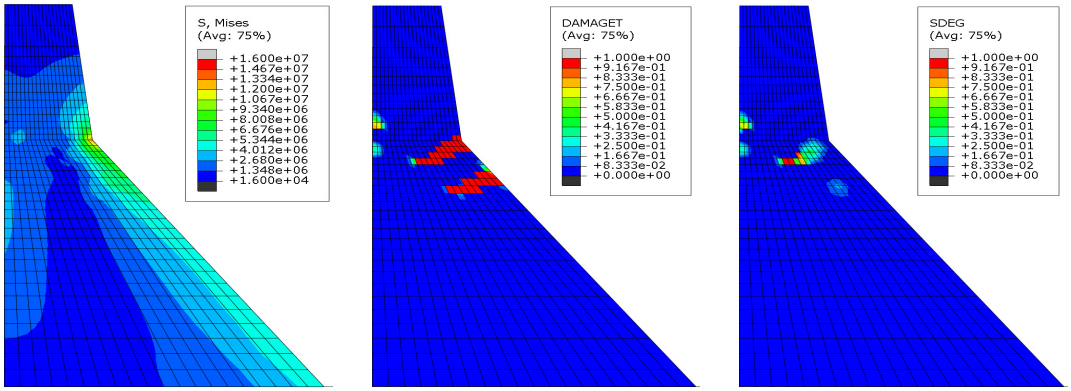

(a) (b) (c)

Figure 6. Peak stress (in Pa) and damage contours of the dam at 4.279 sec for earthquake input with v_{app}= 4000 m/sec: (a) von Mises stress; (b) DAMAGET; (c) SDEG.

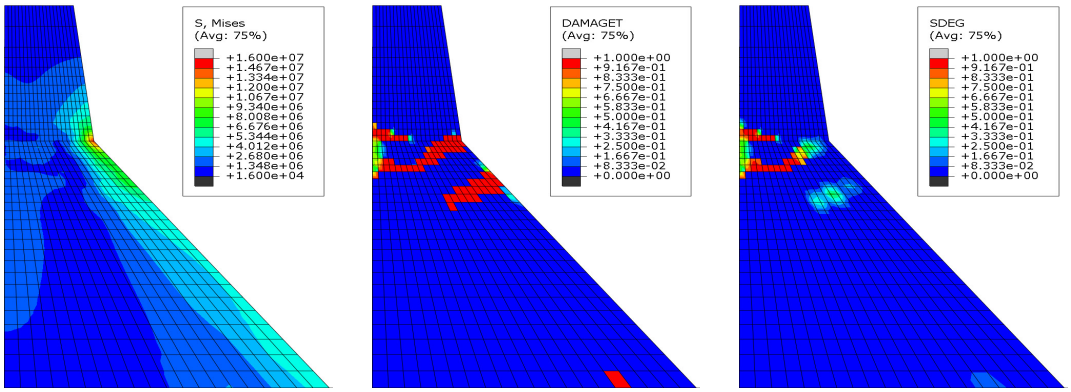

(a) (b) (c)

Figure 7. Peak stress (in Pa) and damage contours of the dam at 4.401 sec for earthquake input with v_{app}= 2000 m/sec: (a) von Mises stress; (b) DAMAGET; (c) SDEG.

base of the neck of the dam on its upstream face. The observed high stress concentrations suggest that cracks may have formed in this vulnerable dam region. The concrete cracking patterns in the dam are clearly demonstrated in parts (b) and (c) of Figs. 5-7, which present the DAMAGET and SDEG damage contours, respectively, for the three excitation cases. DAMAGET and SDEG are Abaqus (2007) classifications for visualizing crack development: In case of no compressive damage, DAMAGET > 0 and SDEG > 0 represent an open crack, whereas DAMAGET > 0 and SDEG = 0 stand for a closed crack. Figures 5-7 indicate that stresses and the degree of damage in the body of the dam increase with decreasing apparent propagation velocity, with a slight increase from the case of uniform input excitation to that of motions propagating with v_{app}= 4000 m/sec, but with a more dramatic one when the motions propagate with the lower apparent velocity of 2000 m/sec. In this latter case, the cracks have penetrated throughout the neck of the dam (Figs. 7(b) and (c)). Another factor that can have considerable impact on the dam response is the contact opening and slipping at the dam-foundation interface. Part (a) of Fig. 8 presents the contact opening at the heel of the dam and part (b) the contact slipping at its toe for the various excitation propagation velocities. The result patterns are similar to those observed earlier in Figs. 4-7. Whereas the contact opening and slipping responses under different excitations share, basically, similar characteristics, i.e. the intermittent "peak" profile for opening and the "step" curve for slipping, the deformations become more pronounced for the lowest apparent propagation velocity. In this case, contact opening (Fig. 8(a)) occurs with higher amplitudes over a longer duration and contact slipping (Fig. 8(b)) is more severe.

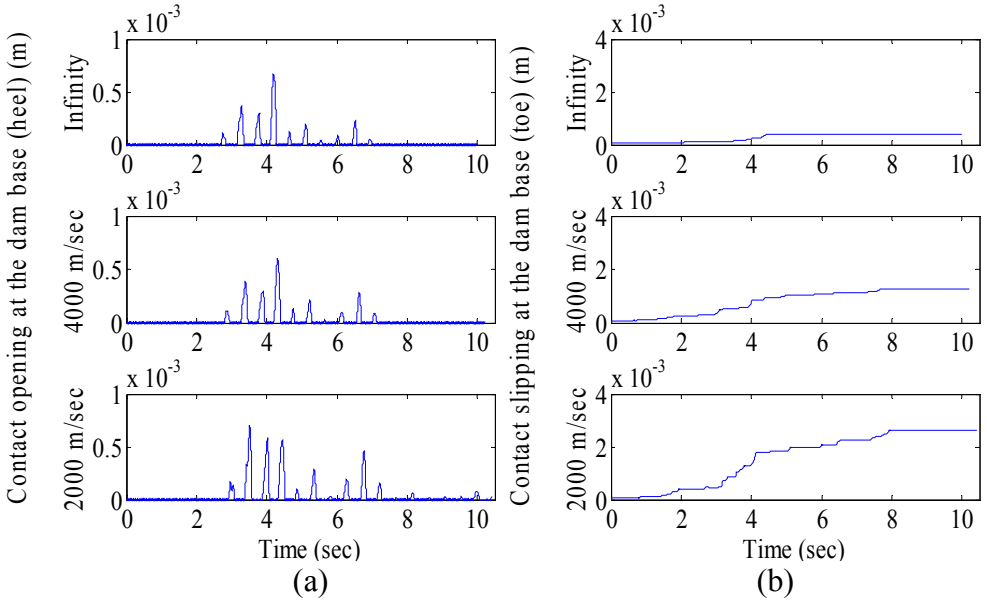

Figure 8. Contact opening, in part (a), and slipping, in part (b), at the dam base for various earthquake input cases.

Conclusions

A nonlinear finite element analysis was utilized to investigate the effect of the spatial variation of seismic ground motions on the response of concrete gravity dams. Features of the numerical model include nonlinearities in the body of the dam and the foundation, contact

interfaces between the fluid-and-solid and solid-and-solid domains, consideration of the reservoir sediment effect, and modeling of the infinite domains. The response of a two-dimensional transverse cross section of the Koyna Dam subjected to spatially variable excitations was then evaluated. The excitation was the 1965 Koyna Earthquake record that was assumed to propagate on the ground surface with an infinite apparent propagation velocity (uniform motions) and two finite ones (4000 and 2000 m/sec). Whereas the results for the higher propagation velocities appear to be similar, a trend of increasing structural response with decreasing propagation velocity was observed, with the slower propagating excitations yielding the highest response and the most severe damage patterns in the structure. Hence, the assumption of uniform motions as input excitations at the base of the structures does not lead to a conservative response for concrete gravity dams.

Acknowledgments

This study was funded, in part, by the US National Science Foundation under Grants CMMI-0647860 and CMMI-0600262. The financial support is gratefully acknowledged.

References

Abaqus, 2007. *Example Problems and Analysis User's Manual*, Version 6.7, Simulia, Dassault Systems, Providence, Rhode Island.

Fenves, G. L., and A. K. Chopra, 1984. Earthquake analysis of concrete gravity dams including reservoir bottom absorption and dam-water-foundation rock interaction, *Earthquake Engineering and Structural Dynamics*, 12 (5), 663-680.

Lee, J., and G. L. Fenves, 1998. Plastic-damage model for cyclic loading of concrete structures, *Journal of Engineering Mechanics*, 124 (8), 892-900.

Leger, P., and M. Boughoufalah, 1989. Earthquake input mechanisms for time-domain analysis of dam-foundation systems, *Engineering Structures*, 11 (1), 37-46.

Lubliner, J., J. Oliver, S. Oller, and E. Oñate, 1989. A plastic-damage model for concrete, *International Journal of Solids and Structures*, 25 (3), 229-326.

Sandler, I. S., 1998. A new computational procedure for wave propagation problems and a new procedure for non-reflecting boundaries, *Computer Methods in Applied Mechanics and Engineering*, 164 (1), 223-233.

Tekie, P. B., and B. R. Ellingwood, 2002. Fragility Analysis of Concrete Gravity Dams, *ERDC/ITL TR-02-6*, Information Technology Laboratory, Engineer Research and Development Center, U.S. Army Corps of Engineers, Washington, D.C.

Zerva, A., 2009. *Spatial variation of seismic ground motions: modeling and engineering applications*, CRC Press, Taylor & Francis Group, Boca Raton, Florida.

Zienkiewicz, O. C., and G. N. Pande, 1977. Time-dependent multilaminate model of rocks - a numerical study of deformation and failure of rock masses, *International Journal for Numerical and Analytical Methods in Geomechanics*, 1 (3), 219-247.